# Synthesis and Self-Assembly of Donor–Acceptor–Donor Based Oligothiophenes and Their Optoelectronic Properties

**ARTICLE** *in* THE JOURNAL OF PHYSICAL CHEMISTRY C · JULY 2011

Impact Factor: 4.77 · DOI: 10.1021/jp204271c



**12 AUTHORS**, INCLUDING:

Raja Siram
Weizmann Institute of Science
**11** PUBLICATIONS **81** CITATIONS
SEE PROFILE

Petr Formanek
Leibniz Institute of Polymer Research Dresden
**63** PUBLICATIONS **752** CITATIONS
SEE PROFILE

Suren A Gevorgyan
Technical University of Denmark
**53** PUBLICATIONS **3,610** CITATIONS
SEE PROFILE

Frederik Christian Krebs
Technical University of Denmark
**453** PUBLICATIONS **22,790** CITATIONS
SEE PROFILE

THE JOURNAL OF PHYSICAL CHEMISTRY C

ARTICLE

pubs.acs.org/JPCC

# Synthesis and Self-Assembly of Donor−Acceptor−Donor Based Oligothiophenes and Their Optoelectronic Properties

Raja Bhaskar Kanth Siram,[†] Kristen Tandy,[∥] Marta Horecha,[‡] Petr Formanek,[‡] Manfred Stamm,[‡] Suren Gevorgyan,[§] Frederik C. Krebs,[§] Anton Kiriy,[‡] Paul Meredith,[∥] Paul L. Burn,[∥] Ebinazar B. Namdas,*[,∥] and Satish Patil*[,†]

[†]Solid State and Structural Chemistry Unit, Indian Institute of Science, Bangalore 560012, India

[‡]Leibniz Institute of Polymer Research, Hohe Strasse 6, 01069, Dresden, Germany

[§]Risø National Laboratory for Sustainable Energy, Technical University of Denmark, Frederiksborgvej 399, DK-4000 Roskilde, Denmark

[∥]Centre for Organic Photonics and Electronics, The University of Queensland, Brisbane, Queensland, Australia 4072

Supporting Information

**ABSTRACT:** In this work, the synthesis of an oligothiophene having a donor−acceptor−donor (D−A−D) chromophore with hydrogen bonding groups is described. The D−A−D molecule was demonstrated to self-organize via intermolecular H-bonding between barbituric acid units. Interactions between the oligothiophene subunits were also found to be important, affording nanoribbons that could be observed by atomic force and transmission electron microscopy. The applicability of the oligothiophene for organic electronic applications was investigated by fabricating organic field-effect transistors (OFETs) and organic photovoltaic devices. The OFET measurements yielded p-type mobility of $7 \times 10^{-7}$ $cm^2/(V\,s)$, and when blended with $C_{60}$-PCBM, the photovoltaic efficiency was observed to be 0.18%.

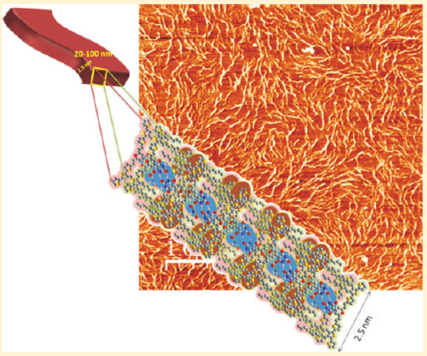

## INTRODUCTION

$\pi$-Conjugated oligomers and particularly oligothiophene-derived molecular systems have been extensively investigated.[1−3] These materials are applied in various optoelectronic devices such as organic field effect transistors,[4,5] organic light emitting diodes[6] and organic photovoltaics.[7−9] The bottom-up approach for optimum performance of such organic optoelectronic devices mainly depends on the ability to molecularly engineer $\pi$-conjugated molecules with size, shape, and functionality to enable self-assembly into desirable morphologies in organic films.[10−12] Polymeric $\pi$-conjugated molecules often self-organize into fibrous nanostructures that are promising as conducting organic nanowires.[13,14] One-dimensional nano-objects with sufficient length and organization are important structures for transport of charges and excitation energies.[15−17] Self-assembly of extended $\pi$- electronic organic molecules using intermolecular noncovalent interactions, such as hydrogen bonding and $\pi-\pi$ stacking interactions, is a powerful strategy in the formation of well-defined nano-objects.[18−22] Recently, a number of oligothiophene-based conjugated materials able to self-assemble into various nanostructures have been reported.[23−26] However, in many of these examples the functional groups responsible for H-bonding were attached at the terminal position thus acting as insulating spacers that are undesirable for optoelectronic devices.[27,28]

In recent years, special attention has been paid to chromophores with a donor−acceptor−donor (D−A−D) structure because of the electronic coupling between the donor and the acceptor through a $\pi$-conjugated bridge. The charge resonance is a characteristic feature of these systems due to a push−pull mechanism.[29] The D−A−D concept has been used for the development of dipolar and quadrapolar molecules for applications in nonlinear optics (NLO),[30] and in recent years $\pi$-conjugated polymers for optoelectronic applications such as organic photovoltaics and organic field-effect transistors.[31] In particular the alternating sequence of electron-donating and electron-accepting aromatic units within a chromophore has been applied to achieve so-called "low band-gap" organic semiconductors.[32] In such chromophores it is proposed that intramolecular charge transfer (ICT) leads to a low energy excitation and a transition dipole in the ground state.

The D−A−D semiconducting polymers have been demonstrated to have high charge carrier mobility in field-effect transistors and good organic solar cell performance.[33,34] Various types of acceptor groups such as perylene bisimide,[35] malononitrile

**Received:** May 8, 2011
**Revised:** June 21, 2011
**Published:** June 22, 2011

**Scheme 1. Synthesis of 5-[2,6-Bis(*E*-2-{3′,4′-di-*n*-hexyl[2,2′:5′,2″-terthiophen]-5-yl}vinyl)-4*H*-pyran-4-ylidene]pyrimidine-2,4,6(1*H*,3*H*,5*H*)-trione (TTB)**

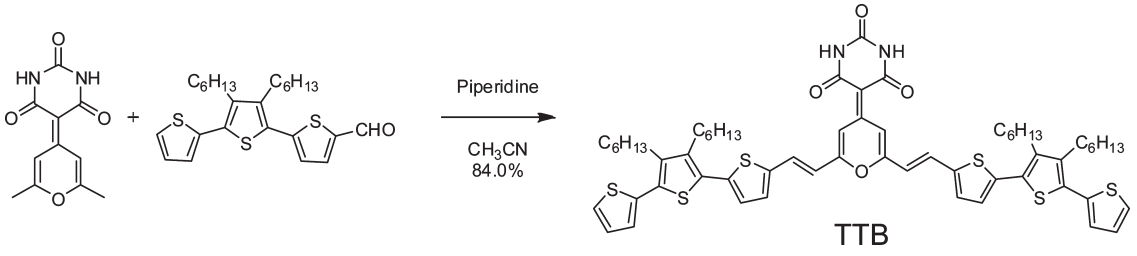


**Scheme 2. Synthetic Pathway for 4 and 5**

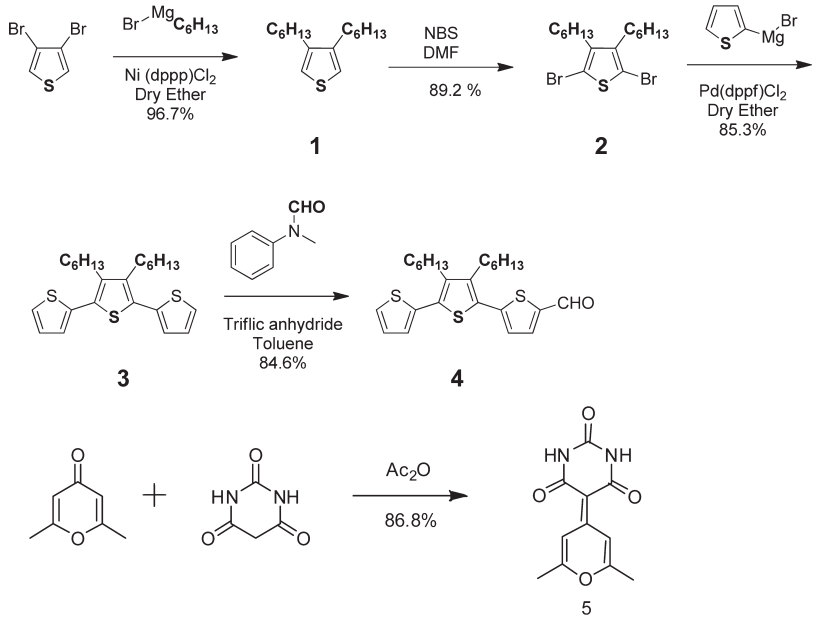


derivatives,[36,37] diketopyrrolopyrrole[38] and benzothiadiazole[39] have been used. In contrast, barbituric acid based D−A−D π-conjugated systems are not known. Herein, we report the first synthesis of the D−A−D derivative composed of a barbituric acid acting as the acceptor and hydrogen bonding moiety with thiophene moieties making up the donor group. The effect of the cooperative hydrogen bonding and π-stacking induced self-assembly on the photophysical properties and the film morphology were investigated. We also report the field-effect mobility and photovoltaic device performance of the new chromophore.

## RESULTS AND DISCUSSION

**Synthesis.** The target molecule, 5-[2,6-bis(*E*-2-{3′,4′-di-*n*-hexyl[2,2′:5′,2″-terthiophen]-5-yl}vinyl)-4*H*-pyran-4-ylidene]-pyrimidine-2,4,6(1*H*,3*H*,5*H*)-trione (TTB), was synthesized by Knoevenagel condensation of 5-(2,6-dimethyl-4*H*-pyran-4-ylidene)pyrimidine-2,4,6-(1*H*,3*H*,5*H*)-trione with the oligothiophene carbaldehyde **4** as shown in Scheme 1.

5-(2,6-Dimethyl-4*H*-pyran-4-ylidene)pyrimidine-2,4,6-(1*H*,-3*H*,5*H*)-trione and the oligothiophene carbaldehyde derivative were synthesized as shown in Scheme 2. All the new derivatives were characterized by $^{1}$H, $^{13}$C NMR, IR Spectra, Mass Spectra and microanalysis. From the $^{1}$H NMR spectrum of compound TTB, the coupling constant ($J$ = 15.7 Hz) of olefinic protons indicates the *E,E*-isomer was obtained in the Knoevenagel condensation reaction. Detailed experimental procedures and characterization of TTB are provided in the Supporting Information.

**Photophysical Properties.** Figure 1 shows the absorption and emission spectra of TTB measured in chloroform and as a thin film at ambient temperature. The UV−visible spectrum of TTB exhibits two absorption bands at 390 and 517 nm. The shorter wavelength band in the UV−visible spectra corresponds to a $\pi-\pi^*$ transition and at the longer wavelength corresponds to an intramolecular charge transfer (ICT) band of the D−A−D system. The absorption features in the thin film undergo a bathochromic shift consistent with planarisation of the chromophore in the solid-state. TTB exhibits emission at $\lambda_{max}$ = 693 nm in chloroform solution and at $\lambda_{max}$ = 733 nm in the solid state.

**Film Morphology.** The thin film morphology of TTB was studied by atomic force microscopy (AFM) and transmission electron microscopy (TEM). TTB possesses good film-forming properties and homogeneously covers substrate surfaces. TTB deposited onto Si-wafers by spin-coating or drop-casting from


dx.doi.org/10.1021/jp204271c |*J. Phys. Chem. C* 2011, 115, 14369–14376

chlorobenzene solution forms many micrometers-long nanoribbons, which are 2.5 nm in height and 20−100 nm in width (Figure 2a). Prior to deposition the TTB solutions were treated with ultrasound and then passed through a membrane filter (pore diameter of 0.2 $\mu$m) in an effort to remove large aggregates. Hence, we believe that the nanoribbon structures were mostly formed during the evaporation of the solvent although some preorganization in the solution cannot be discounted.

It is interesting to note that the nanoribbon morphology was preserved even when TTB and $C_{60}$-PCBM were codeposited (Figure 2d). The formation of the nanoribbons is driven by a combination of forces, van der Waals interactions, $\pi$-stacking and hydrogen bonding. As shown in the schematic in Figure 3, the oligothiophene donor units are responsible for the $\pi$−stacking interactions and the barbituric acid moiety is responsible for the H-bonding interactions. The plausible explanation for the formation of nanoribbons could be the supramolecular interaction among the planar dimeric units (Figure 3a) through $\pi-\pi$ stacking interactions (face-to-face interactions of planar units) along the two dimensions to form a large macroscopic nanoribbon assembly (Figure 3b). The molecular length of the TTB is found to be 2.8 nm which approximates the height of the nanoribbons as observed from AFM. The latter component seems to be of key importance, because many other oligothiophenes that are not capable of hydrogen bonding do not assemble into one-dimensional structures.

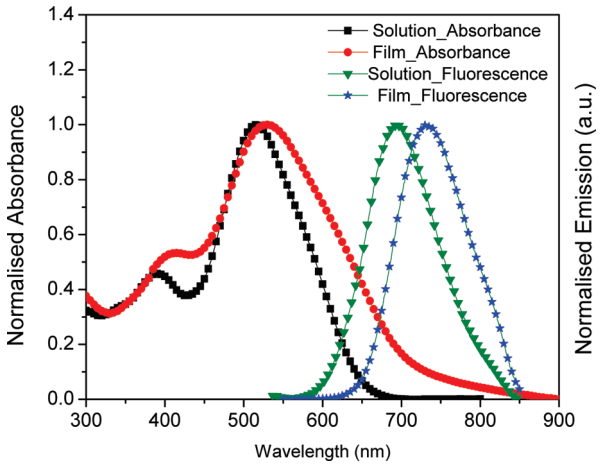


**Figure 1.** UV−visible and fluorescence spectra of TTB in chloroform and as a thin film.

To further elucidate the role of the barbituric acid group, we synthesized the derivative 2-[2,6-bis(*E*-2-{3′,4′-di-*n*-hexyl[2,2′:5′,2″-terthiophen]-5-yl}vinyl)-4H-pyran-4-ylidene]malononitrile[40] (TTM), as shown in Figure 4a, in which malanonitrile has been attached instead of barbituric acid. The surface morphology of this derivative (Figure 4b) was studied by AFM and no nanoribbons were observed. This clearly shows that the intermolecular H-bonding of the barbiturate moieties of the TTB derivative is important for nanoribbon formation. Such nanoribbon architectures could be useful for photovoltaic applications if the TTB molecules within the ribbons were stacked to favor charge and energy transport.

Finally, to further investigate the aggregated behavior of TTB, we recorded the concentration dependent $^1$H NMR spectra (shown in Figure S2, Supporting Information). We observed a downfield shift of the N−H proton as we increased the concentration. These results imply that the N−H proton of barbiturate undergoes intermolecular hydrogen bonding.

**Electrochemical Properties.** Cyclic voltammetry at different scan rates (50, 100, 200, and 500 mV/s) was used to investigate the redox properties of TTB. The oxidation of TTB was measured in dichloromethane (see Figure 5) and a single chemically reversible

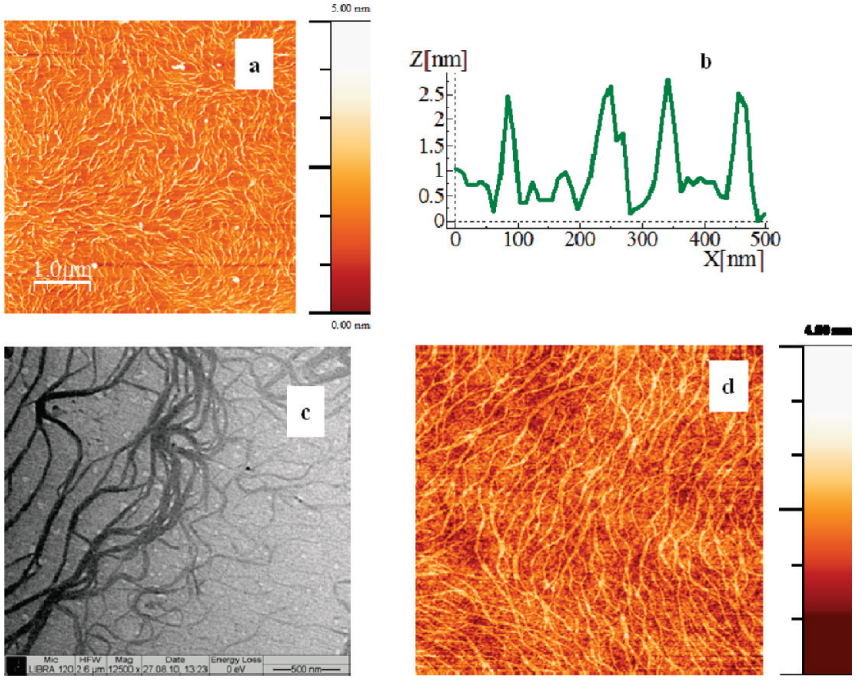


**Figure 2.** AFM 5 $\mu$m × 5 $\mu$m topography image (a) and a cross-sectional profile (b) of film formed by spin-coating a chlorobenzene solution of TTB (4 g/L) onto a silicon wafer. (c) TEM image of nanoribbons formed upon drying of the TTB film. (d) AFM 5 $\mu$m × 5 $\mu$m topography image of a TTB/$C_{60}$-PCBM film deposited on a silicon wafer by spin-coating from chlorobenzene (10 g/L of each component).


dx.doi.org/10.1021/jp204271c |*J. Phys. Chem. C* 2011, 115, 14369–14376

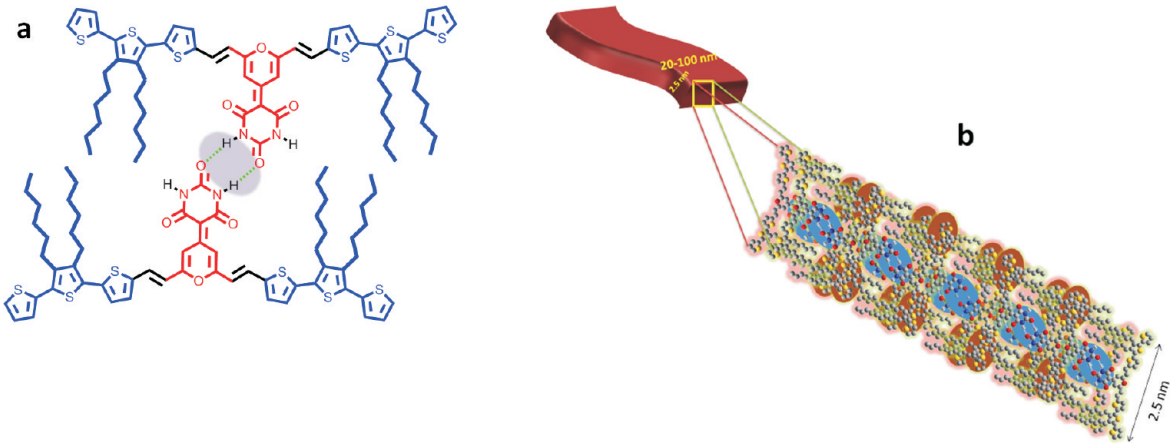


**Figure 3.** Schematic representation of the intermolecular H-bonding (a) and self-assembly of the TTB derivative into nanoribbons (b).

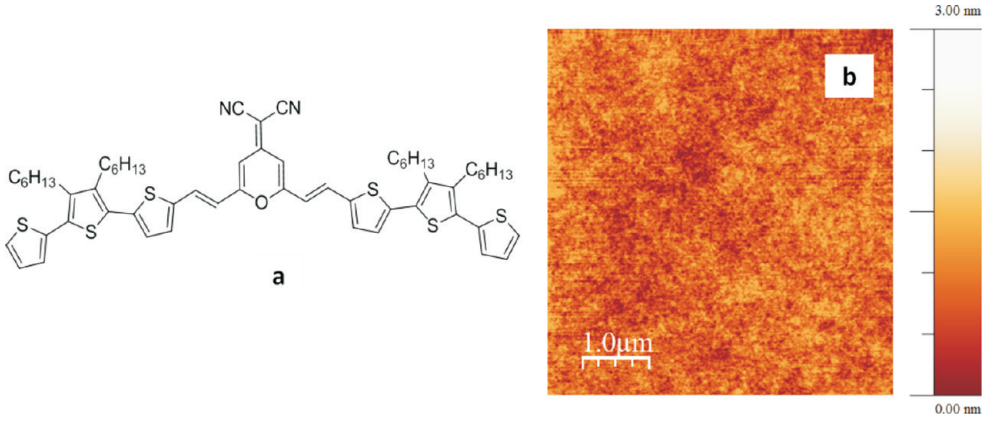


**Figure 4.** (a) Molecular structure of TTM. (b) AFM 5 $\mu$m × 5 $\mu$m topography image of TTM film formed by spin-coating from chlorobenzene (4 g/L) onto a silicon wafer.

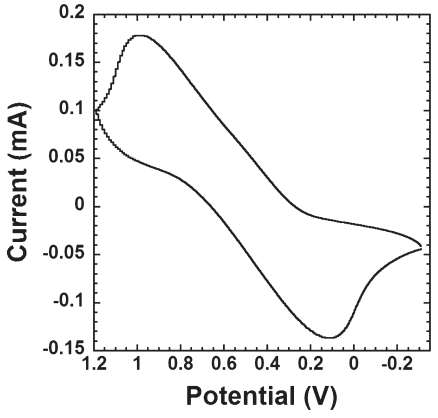


**Figure 5.** Oxidation cyclic voltammagram of TTB in dichloromethane using a scan rate of 100 mV/s and a glassy carbon working electrode.

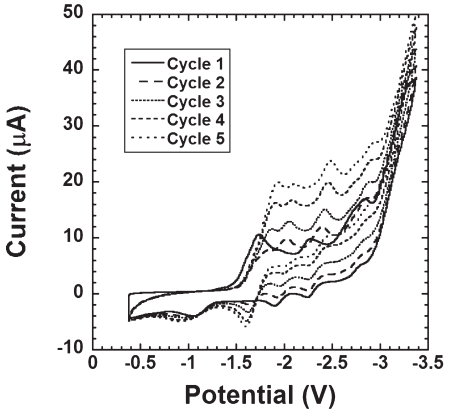


**Figure 6.** Reduction cyclic voltammagram of TTB in tetrahydrofuran using a scan rate of 100 mV/s and a glassy carbon working electrode. The positions of the cathodic peaks shift to more negative potentials as the number of cycles increases.

oxidation with an $E_{1/2}$ of 0.54 V (relative to the ferrocene/ferrocenium couple[41]) was observed independent of scan rate.

The reduction processes were investigated at different scan rates with the TTB dissolved in dry and peroxide free tetrahydrofuran as solvent (see Figure 6). During the measurement the movement in the peaks was seen at all scan rates [50, 100 (Figure 6), 200, and 500 mV/s] although at higher scan rates the resolution of the peaks was lost. One possible explanation for this behavior is that a chemical reaction has taken place. However, during the cycles the new peaks appear to grow and


dx.doi.org/10.1021/jp204271c |J. Phys. Chem. C 2011, 115, 14369–14376

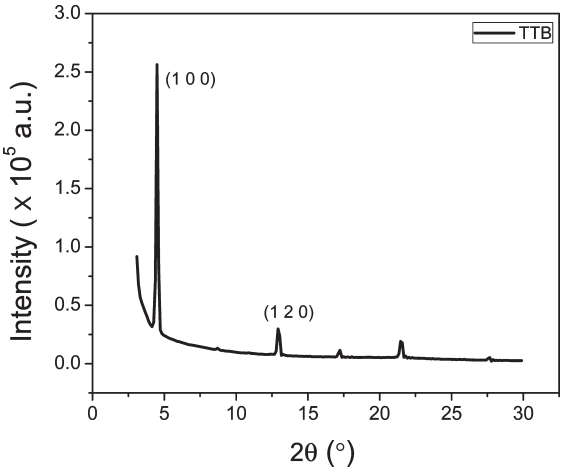


**Figure 7.** Powder X-ray diffraction pattern of a thin film of TTB deposited onto a $SiO_2$ substrate.

stabilize and these results are more consistent with aggregation occurring. Further evidence for aggregation comes from the electrochemical process with an $E_{pa}$ at around −0.9 V. The formation of a peak of this nature has previously been attributed to aggregation in dendrimers.[42] The aggregated species present here is believed to be the same as that in the devices.

The $E_{1/2}$ for the reduction potential of single molecules of TTB in solution was calculated to be −1.61 V, while the $E_{1/2}$ for the reduction potential of the aggregated species was −1.75 V relative to the ferrocenium/ferrocene couple. The reduction potential of the aggregated species was determined using the fifth cycle.

**Powder X-ray Diffraction Pattern.** To study the crystallinity of TTB, the powder X-ray diffraction pattern was recorded. The powder X-ray diffractogram (shown in Figure S3, Supporting Information), reveals the highly crystalline nature of TTB, showing many sharp peaks in both the small angle as well as the wide angle regions. Unfortunately, it was not possible to grow crystals of sufficient quality for single crystal X-ray diffraction experiments. Thin films of TTB were also prepared on a $SiO_2$ substrate by spin-casting from chloroform and drying at 60 °C for 10 min. Figure 7 shows X-ray diffraction pattern for the thin film. Sharp peaks are observed which indicates that the crystalline nature of TTB is retained in a solution processed film.

TTB exhibits distinct diffraction peaks at $2\theta = 4.9°$, 12.9°, and 17.2° with *d*-spacings of 19.6 Å, 6.8 Å, and 5.1 Å, respectively. The first peak can be indexed with a (100) plane, indicating thin film growth along the *a* direction, whereas peak at $2\theta = 12.9°$ arise from the (120) plane. The diffraction peak at $2\theta = 21.5^{o}$ with *d*-spacing 4.1 Å may be due to the $\pi-\pi$ stacking interactions.

**Organic Field-Effect Transistor Measurements.** TTB was tested in a field-effect transistor (FET) to understand more about its charge transport properties. The devices fabricated were a bottom gate-top contact configuration, using $SiO_2$ as the gate dielectric. The electrical characteristics are shown in Figure 8. The output curves show distinct linear and saturation regimes for $I_{DS}$ at low $V_{DS}$ (<−10 V) and high $V_{DS}$ (>−10 V). These results demonstrate hole transport and FET operation in accumulation mode.

The mobility in the saturated regime was extracted using eq 1, where $I_{DS}$ is the source-drain current, $V_G$ is the applied gate voltage, $V_t$ is the threshold voltage of the device, *W* is the channel

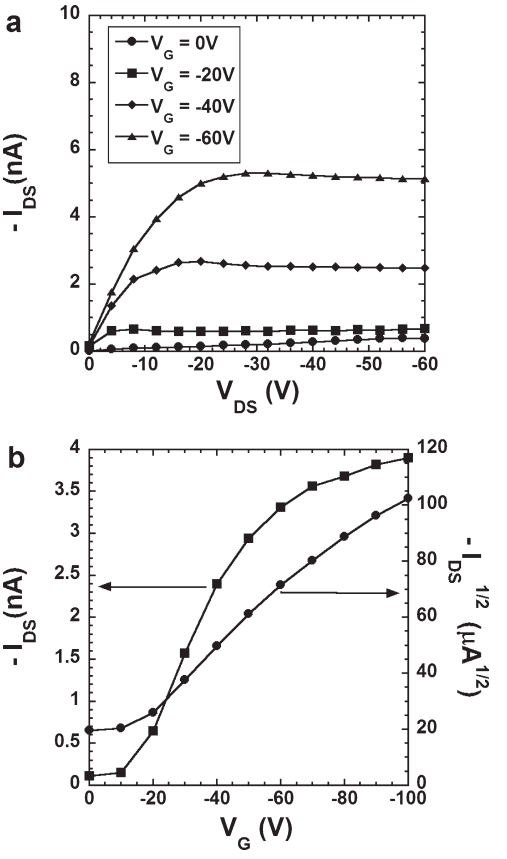


**Figure 8.** Electrical characteristics of a field effect transistor with a TTB active channel. $I_{DS}$ vs $V_{DS}$ sweep (a) transfer curve in the linear regime for $V_{DS} = -10$ V and in the saturation regime for $V_{DS} = -60$ V (b).

width, *L* is the channel length, $C_{ox}$ is the capacitance of the oxide layer, and $\mu_{FE}$ is the field-effect mobility.

$$I_{DS} = \frac{W}{L}\frac{\mu_{FE}C_{ox}}{2}(V_G - V_t)^2 \quad (1)$$

The threshold voltage was extracted in the saturated regime by extrapolating to $I_{DS} = 0$. The ON/OFF ratio was calculated at $V_{DS} = -60$ V and $V_G = 0$ and −60 V. The mobility in the saturated regime was $\sim 7 \times 10^{-7}$ $cm^2/(V\,s)$ and the threshold voltage was approximately −9 V. The low mobility may be due to there being many grain boundaries between the highly ordered regions of the polymer. Due to low currents and mobilities, the ON/OFF ratio was of order $10^2$.

**Organic Photovoltaic Device Measurements.** The photovoltaic properties of TTB were also tested by blending with $C_{60}$−PCBM. A reference poly(3-*n*-hexylthiophene) (P3HT) based device was also prepared.

The device architectures were glass substrate/ITO/PEDOT:PSS/TTB or P3HT:PCBM/aluminum

The devices were characterized using a KHS 575 solar simulator with an AM1.5G spectrum calibrated to 1 sun using a pyranometer. The samples were masked to ensure correct illumination of the active area (~0.5 $cm^2$). The devices were placed under the simulator and *I*−*V* characteristics were measured after the device temperature was stabilized (65 ± 3 °C). Figure 9 shows the *I*−*V* characteristics of the best performing bulk heterojunction devices with the photovoltaic properties summarized in Table 1. The best performance for all the devices


dx.doi.org/10.1021/jp204271c |J. Phys. Chem. C 2011, 115, 14369–14376

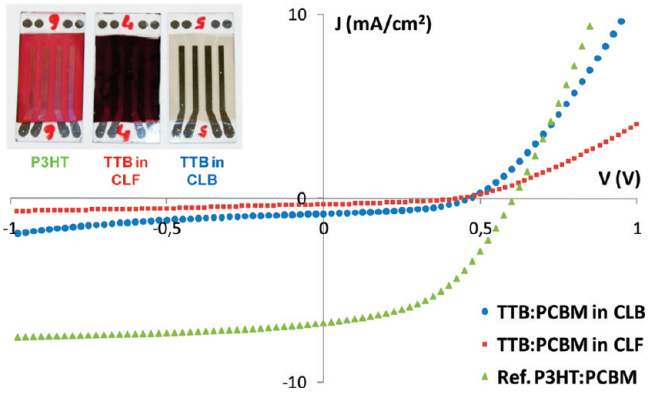


**Figure 9.** *I*−*V* curves of the best performing devices based on TTB:$C_{60}$-PCBM processed from chloroform (red squares) and chlorobenzene (blue circles), and reference P3HT:PCBM (green triangles). Inset: Top view of the devices based on P3HT:PCBM from chlorobenzene (left), and TTB:PCBM from chloroform (CLF) (middle) and chlorobenzene (CLB) (right).

**Table 1. Photovoltaic Parameters for Devices Based on TTB and P3HT**

| device | area ($cm^2$) | $J_{sc}$ ($mA/cm^2$) | $V_{oc}$ (V) | FF (%) | PCE (%) |
|---|---|---|---|---|---|
| TTB in chlorobenzene | 0.5 | 0.84 | 0.47 | 46 | 0.18 |
| TTB in chloroform | 0.5 | 0.32 | 0.43 | 37 | 0.05 |
| P3HT | 0.5 | 6.78 | 0.6 | 46 | 1.85 |

was achieved for the 1:1 ratio of donor:$C_{60}$−PCBM mixtures. A relatively low short circuit current density ($J_{sc}$) of 0.84 $mA/cm^2$ was observed for the best TTB device compared to the 6.78 $mA/cm^2$ of the reference P3HT device. The low current density is ascribed to the fact that the TTB derivative has a much lower hole mobility ($10^{-7}$ $cm^2/(V\,s)$) than P3HT ($10^{-3}$ $cm^2/(V\,s)$).[43]

Figure 9 inset shows the top view of the fabricated devices. From the photograph it is obvious that the device based on the oligomer dissolved in chlorobenzene has low absorption despite the fact that the spin-coating was performed at slow speeds to obtain the thickest films possible. The films of TTB:$C_{60}$−PCBM coated from chloroform solution gave much higher absorbing films although the performance was poorer. Such an effect can be ascribed to differences in film morphology, which will need to be studied further.

**Summary and Prospective.** In summary, we have designed, synthesized and investigated the self-assembly properties of a new D−A−D $\pi$-conjugated oligomer, TTB. The key feature of the TTB design is the central pyran−barbituric acid based moiety, which is involved in the $\pi$-conjugation and acts simultaneously as the electron acceptor and a hydrogen bonding group. We believe that this structural feature is responsible for the high propensity of TTB to self-assemble into nanoribbons under a wide range of deposition conditions including co-deposition with $C_{60}$−PCBM. We also examined the mobility of TTB using an OFET architecture, and the hole mobility was found to be $\sim 7 \times 10^{-7}$ $cm^2/(V\,s)$. When TTB was blended in a 1:1 ratio with $C_{60}$−PCBM, the maximum photovoltaic efficiency was 0.18%. This report reveals that although TTB forms ordered structures within a thin film, the mobility is low and the reason for this needs to be considered when searching for molecular materials that can self-assemble.

Further investigations into the molecular organization of TTB within the nanoribbons as well as the studies of their electrical transport properties and a study on the effect of increased molecular weight (by synthesizing polymers) on the photovoltaic properties are underway.

## EXPERIMENTAL SECTION

**Materials and Methods.** All the solvents were of analytical grade. 3,4-Di-*n*-hexylthiophene[44] and 3′,4′-dihexyl-2,2′:5′,2″-terthiophene[45] were synthesized according to literature procedures. The reported procedure for the synthesis of 3′,4′-di-*n*-hexyl-2,2′:5′,2″-terthiophene has been modified. $^1$H NMR and $^{13}$C NMR spectra were recorded using a Bruker 400 MHz spectrophotometer. Chemical shifts are given in parts per million (ppm) and coupling constants ($J$) in Hertz. The absorption and photoluminescence spectra were characterized using a Perkin-Elmer UV−vis spectrometer and Jobin Yvon Fluorolog 4, respectively. Spectroscopic measurements were performed in standard quartz cells (1 cm × 1 cm). All the measurements were carried out at room temperature.

Electrochemistry measurements were performed using a BAS Epsilon electrochemistry station with a glassy carbon working, $Ag/AgNO_3$ reference electrode in acetonitrile and platinum counter electrodes at a scan rate of 50, 100, 200 and 500 mV/s. Measurements were performed with TTB samples at 1 mM concentration in dichloromethane (HPLC grade) for the oxidation potentials and at 0.5 mM in tetrahydrofuran for the reduction potentials. Dichloromethane was dried over calcium hydride. Tetrahydrofuran was distilled from Na/benzophenone and then dried over lithium aluminum hydride. Tetra-*n*-butylammonium perchlorate at a concentration of 0.1 M was used as the electrolyte. Ferrocene (concentration 1 mM) was used as the standard, with scans run at the same rate and in the same solvent used for TTB. The solutions were deoxygenated with argon before each experiment. In each case, several scans were carried out to confirm the chemical reversibility of the redox process.

Bottom-gate top contact organic field-effect transistors were fabricated and tested in a glovebox under nitrogen. Substrates used were Si, with a silicon oxide layer to act as the gate dielectric. A 350 nm layer of silicon oxide ($SiO_2$) was grown on a heavily doped Si substrate (N++/Az, resistivity 0.001−0.005 ohm/cm, 500 $\mu$m) using an HiTech oxidation furnace to form the gate dielectric. The unpolished side of the Si substrate was etched using hydrofluoric acid to remove the $SiO_2$, followed by sequential deposition of 4 nm of chromium and 50 nm of gold deposited using thermal evaporation to form the gate electrode.

The $SiO_2$ was cleaned in a Class 1000 clean room by sonication in acetone for 20 min, followed by sonication in 2-propanol for 20 min. Substrates were then dried in nitrogen. The $SiO_2$ surface was modified using hexamethyldisilazane (HMDS). An aliquot of 40 $\mu$L was pipetted onto the surface and left to stand for 1 min. Substrates were then spun on a spin-coater at 800 rpm for 60 s. Substrates were then baked on a hot plate for 20 min at 110°. Films were formed by spin-coating a 4 mg/mL solution of TTB in chlorobenzene (>99.9%, anhydrous). The solution was heated to 80 °C prior to spinning and films were spun hot to ensure the material was properly dissolved in solution. Interdigitated gold source and drain electrodes were formed using vacuum evaporation through a shadow mask prepared using deep reactive ion etching.[46] The final thickness of the electrodes was 30 nm, as measured using a quartz crystal monitor during evaporation. The

mask used had a length of 100 $\mu$m and width of 30 mm. OFETs were tested using an Agilent B1500A Semiconductor Device Analyzer and an SA-6 Semi-Auto Prober.

Photovoltaic device preparation was as follows: Glass substrates with a precoated ITO layer (with sheet resistance of about 12 Ω/cm) patterned into four separate stripes were cleaned ultrasonically first 20 min in 2-propanol and then 20 min in demineralized water. An aqueous dispersion of poly(3,4-ethylenedioxythiophene)−poly(styrenesulfonate) (PEDOT:PSS, 1.3 wt % in $H_2O$ as supplied from Aldrich) was deposited onto the glass/ITO substrate by spin-coating at 2800 rpm followed by annealing of the substrates for 5 min at 150 °C. The active layer of the tested material was prepared by mixing TTB with PCBM in different ratios, including 2:1, 1:2, and 1:1 and dissolving the mixture using chlorobenzene, chloroform, or a mixture of these two (1:1 ratio). The solution was filtered with a 1 $\mu$m PVDF filter prior to spin-coating. The active solution of the reference device was prepared by mixing P3HT with $C_{60}$−PCBM at a 10:9 ratio in chlorobenzene. The active layer was formed by spin-coating at different spin speeds to obtain different film thicknesses. Finally, an aluminum electrode was thermally evaporated on top of the device. The reference P3HT device was additionally annealed at 150 °C for 5 min after the aluminum evaporation.

**Synthesis of 5-[2,6-Bis(*E*-2-{3′,4′-di-*n*-hexyl[2,2′:5′,2″-terthiophen]-5-yl}vinyl)-4*H*-pyran-4-ylidene]pyrimidine-2,4,6-(1*H*,3*H*,5*H*)-trione (TTB).** Piperidine (1 mL) was added to a mixture of 5-(2,6-dimethyl-4*H*-pyran-4-ylidene)pyrimidine-2,4,6-(1*H*,3*H*,5*H*)-trione (70.5 mg, 0.3 mmol,1 equiv) and **4** (267.5 mg, 0.6 mmol, 2 equiv) that was held under argon. The mixture was heated at reflux for ∼24 h and the reaction mixture cooled to room temperature and filtered. The precipitate was washed with acetonitrile and then dried under vacuum to give TTB (274 mg, 84%).

$^1$H NMR (400 MHz, $CDCl_3$): $\delta$ 8.89 (s, 2H), 7.66 (d, $J$ = 15.6 Hz, 2H), 7.35 (d, $J$ = 5.2 Hz, 2H), 7.29 (d, $J$ = 4.0 Hz, 2H), 7.17 (d, $J$ = 3.2 Hz, 2H), 7.14 (d, $J$ = 3.6 Hz, 2H), 7.09 (t, $J$ = 4.8 Hz, 2H), 6.69 (d, $J$ = 15.6 Hz, 2H), 2.79 (t, $J$ = 7.6 Hz, 4H), 2.72 (t, $J$ = 7.6 Hz, 4H), 1.73−1.26 (m, 32H), 0.95 (t, $J$ = 6.8 Hz, 6H), 0.90 (t, $J$ = 6.8 Hz, 6H).

$^{13}$C NMR (100 MHz, $CDCl_3$): $\delta$ 164.6, 160.6, 141.5, 140.6, 140.3, 139.5, 135.8, 131.5, 131.3, 130.3, 129.3, 127.5, 126.5, 126.2, 125.7, 118.0, 111.8, 31.5, 31.4, 30.7, 30.5, 29.6, 29.5, 28.4, 28.1, 22.6, 14.1, 14.0.

IR spectrum: 3190.1, 2925.8, 2854.3, 1713.6, 1618.4, 1602.6, 1535.1, 1441.5, 1358.5, 1180.4, 1063.8, 951.9 $cm^{-1}$.

Mass spectra: found, 1087.879 $(M + H)^+$; calculated, 1087.610 $(M + H)^+$.

Microanalysis Calculated for $C_{61}H_{70}N_2O_4S_6$: C, 67.36; H, 6.49; N, 2.58; S, 17.69. Found: C, 67.45; H, 6.36; N, 3.04; S, 17.51.

## ■ ASSOCIATED CONTENT

**Supporting Information.** Characterization data for all new compounds and experimental protocols as well as optical data and NMR data. This material is available free of charge via the Internet at http://pubs.acs.org.

## ■ AUTHOR INFORMATION

### Corresponding Author

*E.B.N.: e-mail, e.namdas@uq.edu.au. S.P.: tel, +91-80- 22932651; fax, +91-80-23601310; e-mail, satish@sscu.iisc.ernet.in.

## ■ ACKNOWLEDGMENT

S.P. thanks ISRO-IISc Space Technology Cell for supporting this work through the project ISTC/CSS/STP/252. R.B.K.S. thanks CSIR for Senior Research Fellowship and A.K. thanks DFG for financial support (KI-1094/3-1 and KI-1094/4-1). P.L.B. is an Australian Research Council Federation Fellow and P.M. a University of Queensland Vice Chancellors Senior Research Fellow. The Centre for Organic Photonics and Electronics is a strategic initiative of the University of Queensland, and we also acknowledge use of equipment through the Australian Nanofabrication Facility Queensland Node.

## ■ REFERENCES

(1) Mishra, A.; Ma, C.; Bauerle, P. *Chem. Rev.* **2009**, *109*, 1141–1276.
(2) Cremer, J.; Briehn, C. A. *Chem. Mater.* **2007**, *19*, 4155–4165.
(3) Radke, K. R.; Ogawa, K.; Rasmussen, S. C. *Org. Lett.* **2005**, *7*, 5253–5256.
(4) Garnier, F.; Hajlaoui, R.; Yassa, A.; Srivastava, P. *Science* **1994**, *265*, 1684–1688.
(5) Ohshita, J.; Izumi, Y.; Kim, D.; Kunai, A.; Kosuge, T.; Kunugi, Y.; Naka, A.; Ishikawa, M. *Organometallics* **2007**, *26*, 6150–6154.
(6) Burroughes, J. H.; Bradley, D. D. C; Brown, A. R.; Marks, R. N.; Mackay, K.; Friend, R. H.; Burns, P. L.; Holmes, A. B. *Nature* **1990**, *347*, 539–540.
(7) Liang, Y.; Feng, D.; Wu, Y.; Tsai, S. T.; Li, G.; Ray, C.; Yu, L. *J. Am. Chem. Soc.* **2009**, *131*, 7792–7799.
(8) Park, S. H.; Roy, A.; Beaupre, S.; Cho, S.; Coates, N.; Moon, J. S.; Moses, D.; Leclerc, M.; Lee, K.; Heeger, A. J. *Nat. Photonics* **2009**, *3*, 297–302.
(9) Hains, A.; Liang, Z.; Woodhouse, M.; Gregg, B. *Chem. Rev.* **2010**, *110*, 6689–6735.
(10) Hoeben, F. J. M.; Jonkheijm, P.; Meijer, E. W.; Schenning, A. P. H. J. *Chem. Rev.* **2005**, *105*, 1491–1546.
(11) Schenning, A. P. H. J.; Meijer, E. W. *Chem. Commun.* **2005**, 3245–3248.
(12) Ajayaghosh, A.; Praveen, V. K. *Acc. Chem. Rev.* **2007**, *40*, 644–656.
(13) Schenning, A. P. H. J.; Jonkheijm, P.; Hoeben, F. J. M.; Van Herrikhuyzen, J.; Meskers, S. C. J.; Meijer, E. W.; Herz, L. M.; Daniel, C.; Silva, C.; Phillips, R. T.; et al. *Synth. Met.* **2004**, *147*, 43–48.
(14) Kiriy, N.; Jähne, E.; Adler, H.−J.; Schneider, M.; Kiriy, A.; Gorodyska, G.; Minko, S.; Jehnichen, D.; Simon, P.; Fokin, A. A.; et al. *M. Nano Lett.* **2003**, *3*, 707–712.
(15) Hoeben, F. J. M.; Jonkheijm, P.; Meijer, E. W.; Schenning, A. P. H. J. *Chem. Rev.* **2005**, *105*, 1491–1546.
(16) Schenning, A. P. H.; Meijer, E. W. *Chem. Commun.* **2005**, 3245–3258.
(17) Grimsdale, A. C.; Mullen, K. *Angew. Chem., Int. Ed.* **2005**, *44*, 5592–5629.
(18) Schoonbeek, F. S.; van Esch, J. H.; Wegewijs, B.; Rep, D. B. A.; de Haas, M. P.; Klapwijk, T. M.; Kellogg, R. M.; Feringa, B. L. *Angew. Chem., Int. Ed.* **1999**, *38*, 1393–1397.
(19) Messmore, B. W.; Hulvat, J. F.; Sone, E. D.; Stupp, S. I. *J. Am. Chem. Soc.* **2004**, *126*, 14452–14458.
(20) Guerzo, A. D.; Olive, A. G. L.; Reichwagen, J.; Hopf, H.; Desvergne, J.-P. *J. Am. Chem. Soc.* **2005**, *127*, 17984–17985.
(21) Praveen, V. K.; George, S. J.; Varghese, R.; Vijayakumar, C.; Ajayaghosh, A. *J. Am. Chem. Soc.* **2006**, *128*, 7542–7550.
(22) Kiriy, N.; Bocharova, V.; Kiriy, A.; Stamm, M.; Krebs, F. C.; Adler, H.-J. *Chem. Mater.* **2004**, *16*, 4765–4771.
(23) Prasanthkumar, S.; Saeki, A.; Seki, S; Ajayaghosh, A. *J. Am. Chem. Soc.* **2010**, *132*, 8866–8867.
(24) Yagai, S.; Kubota, S.; Saito, H.; Unoike, K.; Karatsu, T.; Kitamura, A.; Ajayaghosh, A.; Kanesato, M.; Kikkawa, Y. *J. Am. Chem. Soc.* **2009**, *131*, 5408–5410.

(25) Schmid, S.; Mena-Osteritz, E.; Kopyshev, A.; Bauerle, P. *Org. Lett.* **2009**, *11*, 5098–5101.
(26) Kiriy, N.; Kiriy, A.; Bocharova, V.; Stamm, M.; Richter, S.; Plötner, M.; Fischer, W.-J.; Krebs, F. C.; Senkovska, I.; Adler, H.-J. *Chem. Mater.* **2004**, *16*, 4757–4764.
(27) Leclere, Ph.; Surin, M.; Viville, P.; Lazzaroni, R.; Kilbinger, A. F. M.; Henze, O.; Feast, W. J.; Cavallini, M.; Biscarini, F.; Schenning, A. P. H. J.; et al. *Chem. Mater.* **2004**, *16*, 4452–4466.
(28) Yagai, S.; Mahesh, S.; Kikkawa, Y.; Unoike, K.; Karatsu, T.; Kitamura, A.; Ajayaghosh, A. *Angew. Chem., Int. Ed.* **1999**, *47*, 4691–4694.
(29) Painelli, A.; Terenziani, F. *J. Phys. Chem. A* **2000**, *104*, 11041–11048.
(30) Yao, S.; Ahn, H.-Y.; Wang, H.; Fu, J.; Stryland, E. W. V.; Hagan, D. J.; Belfield, K. D. *J. Org. Chem.* **2010**, *75*, 3965–3974.
(31) Sonar, P.; Singh, S. P.; Sudhakar, S.; Dodabalapur, A.; Sellinger, A. *Chem. Mater.* **2008**, *20*, 3184–3190.
(32) Schulze, K.; Uhrich, C.; Schüppel, C.; Leo, K.; Pfeiffer, K.; Brier, E.; Reinold, E.; Bäuerle, P. *Adv. Mater.* **2006**, *18*, 2872–2875.
(33) Mi, Y. C.; Su, J. K.; Yoon, D. H.; Dong, H. P.; Kyung, H. K.; Dong, H. C.; Jinsoo, J. *Adv. Funct. Mater.* **2008**, *18*, 2905–2909.
(34) Fabio, S.; Michael, D. I.; Luca, B.; Antonio, F.; Giorgio, A. P.; Tobin, J. M. *J. Am. Chem. Soc.* **2008**, *130*, 17640–17641.
(35) Chen, S.; Liu, Y.; Qiu, W.; Sun, X.; Ma, Y.; Zhu, D. *Chem. Mater.* **2005**, *17*, 2208–2215.
(36) Xue, L.; He, J.; Gu, X.; Yang, Z.; Xu, B.; Tian, W. *J. Phys. Chem. C* **2009**, *113*, 12911–12917.
(37) Li, Y.; Xue, L.; Li, H.; Li, Z.; Xu, B.; Wen, S.; Tian, W. *Macromolecules* **2009**, *42*, 4491–4499.
(38) Walker, B.; Tamayo, A. B.; Dang, X; Zalar, P.; Seo, J. H.; Garcia, A.; Tantiwiwat, M.; Nguyen, T. *Adv. Funct. Mater.* **2009**, *19*, 3063–3069.
(39) Akhtaruzzaman, Md.; Tomura, M.; Zaman, Md. B.; Nishida, J.; Yamashita, Y. *J. Org. Chem.* **2002**, *67*, 7813–7818.
(40) Li, Z.; Pei, J.; Li, Y.; Xu, B.; Deng, M.; Liu, Z.; Li, H.; Lu, H.; Li, Q.; Tian, W. *J. Phys. Chem. C* **2010**, *114*, 18270–18278.
(41) Gritzner, G.; Kuta, J. *Electrochim. Acta* **1984**, *29*, 869–873.
(42) Beavington, R.; Frampton, M. J.; Lupton, J. M.; Burn, P. L.; Samuel, I. D. W. *Adv. Funct. Mater.* **2003**, *13*, 211–218.
(43) Bao, Z.; Dodabalapur, A.; Lovinger, A. *J. Appl. Phys. Lett.* **1996**, *69*, 4108–4110.
(44) Banishoeib, F.; Henckens, A.; Fourier, S.; Vanhooyland, G.; Breselge, M.; Manca, J.; Cleij, T. J.; Lutsen, L.; Vanderzande, D.; Nguyen, L. H.; et al. *Thin Solid Films* **2008**, *516*, 3978–3988.
(45) Diaz-Quijada, G. A.; Weinberg, N.; Holdcroft, S.; Pinto, B. M. *J. Phys. Chem. A* **2002**, *106*, 1266–1276.
(46) Aljada, M.; Mutkins, K.; Vamvounis, G.; Burn, P.; Meredith, P. *J. Micromech. Microeng.* **2010**, *20*, 075037.